Green Chemistry

PAPER

View Article Online
View Journal | View Issue

Cite this: *Green Chem.*, 2025, **27**, 10673

Integration of metabolic and bioprocess engineering for the production of β-ketoadipic acid from glucose and xylose by *Pseudomonas putida*

Gabriel M. Rubinstein, [a,b] Sekgetho C. Mokwatlo, [a,b] Louis Chirban,[a] Ariel R. Lepard, [a] Morgan A. Ingraham, [a,b] Kelsey J. Ramirez, [a,b] Hoon Choi, [a] Patrick O. Saboe, [c] Davinia Salvachúa, [a,b] Christopher W. Johnson [a,b] and Gregg T. Beckham *[a,b]

Received 11th April 2025,
Accepted 31st July 2025

DOI: 10.1039/d5gc01813g

rsc.li/greenchem

β-Ketoadipic acid is a common intermediate in aerobic microbial aromatic catabolism that can be used as a monomer in performance-advantaged biopolymers. Here, we engineered *Pseudomonas putida* KT2440 to produce β-ketoadipate from glucose and xylose, the most prevalent carbohydrates derived from lignocellulosic polysaccharides. With the top-performing strain, *P. putida* GR038, we conducted bioprocess development using glucose and xylose as substrates in a 2 : 1 molar ratio to mimic lignocellulosic hydrolysate. Fed-batch cultivations achieved a titer of 65.8 g L^{-1} and a rate of 0.69 g L^{-1} h^{-1}, with a C-mol yield of 0.52. Application of adsorptive *in situ* product recovery further improved the effective titer to 92.0 g L^{-1} and the rate to 0.83 g L^{-1} h^{-1}, while also improving the downstream purity of β-ketoadipate from 88.3 wt% to 99.0 wt%. These results show promise towards industrial production of β-ketoadipate from lignocellulosic sugars.

Green foundation

1. This work demonstrates integrated metabolic engineering, bioprocess development, and adsorptive separations to substantially improve the production of a bio-based chemical for performance-advantaged bioproducts.
2. The co-utilization of glucose and xylose in a β-ketoadipic acid production strain enables higher overall product yields from lignocellulosic hydrolysates, and the incorporation of *in situ* product recovery enables higher product (effective) titers and rates.
3. Further metabolic engineering and bioprocess development, coupled to improved separation processes, could further the applicability of this approach.

β-Ketoadipic acid (βKA) is a C6 diacid intermediate in aerobic microbial aromatic catabolic pathways downstream of oxidative ring-opening reactions from catechol, protocatechuic acid (PCA), hydroxyquinol, and methoxyhydroquinone.[1–4] When substituted for adipic acid, a petroleum-derived monomer, in the production of nylon, βKA imparts performance-advantaged properties while lowering manufacturing energy demand, making it an attractive target molecule.[5–7] The Gram-negative soil bacterium *Pseudomonas putida* KT2440 (hereafter *P. putida*) is a promising host to produce βKA, as it natively metabolizes glucose and lignin-related aromatic compounds, which are both components of lignocellulose, its metabolism includes the βKA pathway in which βKA is an intermediate,[8] and it exhibits inherently high toxicity tolerance, making it amenable to industrially relevant cultivations.[9–11]

P. putida has been engineered to generate βKA from aromatic feedstocks – including PCA,[12] 4-hydroxybenzoic acid,[5] black liquor from pulp production,[13] hydroxycinnamic acids from corn stover,[14] mixed plastic waste streams following chemical oxidation,[15] and terephthalic acid liberated from PET glycolysis[16] – and a single sugar, glucose. For the production of βKA from glucose, we previously reported an engineered strain of *P. putida* that converts glucose to βKA at 26.0 g L^{-1}, 0.09 g L^{-1} h^{-1}, and yield of 0.36 C-mol βKA/C-mol glucose.[6] However, lignocellulosic feedstocks typically comprise

[a]*Renewable Resources and Enabling Sciences Center, National Renewable Energy Laboratory, Golden, CO 80401, USA. E-mail: gregg.beckham@nrel.gov*
[b]*Agile BioFoundry, Emeryville, CA 94608, USA*
[c]*Strategic Energy Analysis Center, National Renewable Energy Laboratory, Golden, CO 80401, USA*

cellulose and hemicellulose which, after enzymatic hydrolysis, predominantly release glucose and xylose.[17] Metabolic co-utilization of these sugars enables use of lignocellulosic feedstocks, which can potentially exhibit a lower environmental impact relative to first-generation sugar feedstocks.[18] Xylose utilization by engineered *P. putida* has been previously demonstrated, including for the production of *cis*,*cis*-muconic acid (hereafter muconic acid), another intermediate in the βKA pathway, by the heterologous expression of both the xylose isomerase pathway (*xylAB*, *xylE*) and the pentose phosphate pathway (PPP) genes transaldolase (*talB*) and transketolase (*tktA*) from *Escherichia coli*, among other genetic modifications.[19–27]

The minimum selling price of βKA produced from carbohydrates *via* microbial conversion depends on bioprocess performance metrics, including titer, rate, and yield.[6] The integration of *in situ* product recovery (ISPR) systems with bioreactor cultivations, for continuous product separation to reduce end-product inhibition, has improved performance metrics in multiple bioprocesses.[28,29] For instance, extractive or adsorptive ISPR has been demonstrated to improve production of several value-added, bio-based products, including diacids such as itaconic acid,[30,31] muconic acid,[32] malic acid,[33] succinic acid,[34] and fumaric acid.[35,36] When carboxylic acids are selectively removed from the cultivation broth *via* adsorptive ISPR, an adsorption column containing activated carbon or anion-exchange resin is used.[31,34–38] Adsorptive ISPR to enhance carboxylic acid production by *P. putida* has been demonstrated with perillic acid.[39]

Herein, we report metabolic engineering of *P. putida* for the generation of βKA from glucose and xylose. βKA production by the top-performing strain, GR038, was demonstrated in shake flasks and bioprocess optimization was performed in bioreactors in batch and fed-batch modes. Subsequently, adsorptive ISPR was implemented with fixed-bed anion-exchange columns to continuously remove βKA during its production in bioreactors in fed-batch mode, which considerably improved both the productivity and effective titer. Moreover, the βKA isolated from adsorptive ISPR showed higher purity compared to βKA isolated from fed-batch cultivations without ISPR, establishing a process improvement over a previously developed post-cultivation purification strategy.[6] The metabolic and bioprocess optimizations developed in this study represent substantial progress in manufacturing this molecule for the production of performance-advantaged polymers.

Results

Metabolic engineering to repurpose a muconic acid production *P. putida* strain for βKA production

For the generation of βKA from sugars, metabolic engineering was undertaken to repurpose a muconic acid production strain of *P. putida* (LC224) capable of co-utilizing glucose and xylose.[24,27] The aim of these genetic modifications was to convert carbon from glucose and xylose to βKA, and to facilitate product accumulation by disrupting the native catabolic pathway between βKA and the TCA cycle (Fig. 1). Strains of *P. putida* utilized or generated in this study are listed in Table 1.

Repurposing LC224 to produce βKA began with the restoration of the native genes encoding the protocatechuate 3,4-dioxygenase (*pcaHG*), which converts PCA to 3-carboxy-*cis*,*cis*-muconic acid (Fig. 1). To route carbon from PCA to muconic acid, the *pcaHG* genes were previously deleted;[24] restoration of *pcaHG* re-established the native pathway from PCA to the TCA cycle (*via* βKA), generating strain GR011. During growth on glucose, this strain displayed a shorter lag phase and higher final biomass accumulation (measured by OD_{600}) than LC224 (Fig. 1 and Fig. S1).

In wild-type *P. putida*, muconic acid derived from catechol is assimilated into central carbon metabolism through CatB and CatC, a muconate cycloisomerase and muconolactone isomerase, respectively. Together, these enzymes convert muconic acid to βKA. To enable the accumulation of muconic acid, these genes were deleted in LC224, along with the transcriptional activator encoded by *catR*, which regulates their expression.[24,40] While not required for βKA production in a pathway that proceeds through 3-carboxy-*cis*,*cis*-muconic acid rather than muconic acid, the native *catRBCA* locus was restored to avoid over-engineering in the GR011 background, yielding strain GR014 (Fig. S1). Generation of muconic acid from glucose and xylose in LC224 was facilitated by the heterologous expression of *aroY* and *ecdB* from *Enterobacter cloacae* integrated into the *pykA* locus. The protocatechuate decarboxylase, AroY, catalyzes the conversion of PCA to catechol, while EcdB catalyzes the synthesis of the prenylated-FMN cofactor requisite for AroY activity.[41,42] Deletion of *aroY* and *ecdB* in GR014 abolished production of muconic acid, ensuring that carbon flux through PCA was routed toward βKA in strain GR017 (Fig. S1).

In native *P. putida* metabolism, the penultimate step of the βKA pathway is the addition of a CoA group to βKA, which is subsequently cleaved to generate succinate and acetyl-CoA for growth (Fig. 1). Together, *pcaIJ* encode the βKA-CoA transferase complex and deletion of these genes prevents βKA catabolism.[12] Deletion of *pcaIJ* from GR017 produced GR020, in which the accumulation of βKA was observed in shake flasks (Fig. 2A). Specifically, the conversion of 6.2 g L^{-1} glucose and 2.6 g L^{-1} xylose by GR020 generated 2.9 ± 0.03 g L^{-1} βKA in 37 h. An increase in lag time and decrease in the final OD_{600} were observed in strain GR020 (and all subsequent strains) relative to GR017, due to the uncoupling of βKA and the TCA cycle (Fig. 1 and Fig. S1). Relative to LC224, GR020 displayed a higher final OD_{600} (3.0 *vs.* 2.4), completely consuming all glucose and xylose by 37 h (Fig. 2A and Fig. S2). During growth on 5.4 g L^{-1} glucose in a 96-well plate monitored with a BioScreen C Pro (Growth Curves USA), strains GR011, GR014, and GR017 displayed analogous growth phenotypes, while LC224 and strains in which *pcaIJ* were deleted displayed a roughly 12 h increase in lag phase (Fig. S1).

P. putida harbors a combination of Entner–Doudoroff (ED), Embden–Meyerhof–Parnas (EMP), and PPP, where EMP

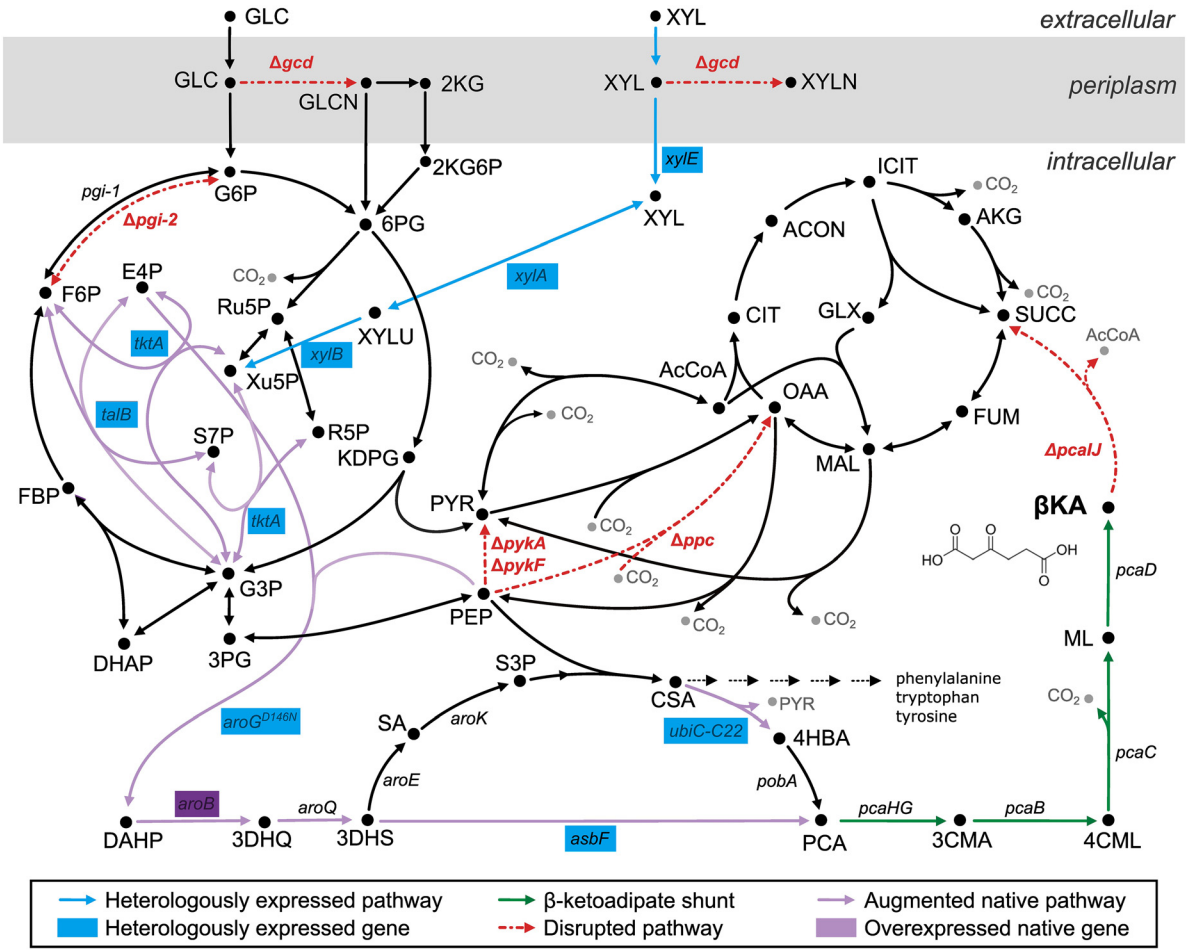

Fig. 1 Metabolic pathway for the conversion of glucose and xylose to βKA in *P. putida* KT2440 strain GR038. Carbon from glucose and xylose is directed from the Entner–Doudoroff–Embden–Meyerhof–Parnas (EDEMP) cycle to the shikimate pathway by the condensation of erythrose 4-phosphate (E4P) and phosphoenolpyruvate (PEP). Assimilation of PEP into the TCA cycle *via* pyruvate (PYR) or oxaloacetate (OAA) is prevented by the deletion of the native genes *pykA*, *pykF*, and *ppc*. Carbon in the shikimate pathway is directed to PCA by two pathways, relying on the heterologous expression of *ubiC-C22* from *E. coli* and *asbF* from *Bacillus cereus*. The accumulation of βKA is enabled by the deletion of the *pcaIJ* genes to prevent reassimilation of carbon into the TCA cycle as succinate (SUCC). The target molecule for production, βKA, is labeled in bold, and its chemical structure is shown. A full list of abbreviations for gene and metabolite names is provided in Table S1.

Table 1 Strains used in this study

Strain	Genotype	Ref.
LC224	***P. putida* KT2440** Δ*catRBCA*::P_{tac}:*catA* Δ*pcaHG*::P_{tac}:*aroY:ecdB:asbF* Δ*pykA::aroG-D146N:aroY:ecdB:asbF* Δ*pgi-2* Δ*ppc* Δ*gcd* Δ*ampC::xylE*$_{A455V\wedge A62V}$*:xylAB:tktA:talB PP_2834*:P_{lac}:*ubiC-C22:PP_2835* Δ*hexR* G→A at P_{PP_2569} Δ*pykF*::P_{tac}:*aroB*	33
GR011	**LC224** restoration of *pcaHG*	This study
GR014	**GR011** restoration of *catRBCA*	This study
GR017	**GR014** Δ*aroY:ecdB* from Δ*pykA* locus	This study
GR020	Δ*pykA::aroG-D146N:asbF* Δ*pgi-2* Δ*ppc* Δ*gcd* Δ*ampC::xylE*$_{A455V\wedge A62V}$*:xylAB:tktA:talB PP_2834*:P_{lac}:*ubiC-C22:PP_2835* Δ*hexR* G→A at P_{PP_2569} Δ*pykF*::P_{tac}:*aroB* Δ*pcaIJ*	This study
GR023	**GR020** Δ*pgi-1*	This study
GR029	**GR023** Δ*lvaE*	This study
GR032	**GR029** Δ*gacS*	This study
GR038	Δ*pykA::aroG-D146N:asbF* Δ*pgi-2* Δ*ppc* Δ*gcd* Δ*ampC::xylE*$_{A455V\wedge A62V}$*:xylAB:tktA:talB PP_2834*:P_{lac}:*ubiC-C22:PP_2835* Δ*hexR* G→A at P_{PP_2569} Δ*pykF*::P_{tac}:*aroB* Δ*pcaIJ* Δ*gacS* Δ*lvaE*	This study

enzymes operate in the gluconeogenic direction and ED enzymes operate in the glycolytic direction[10] (Fig. 1). To prevent carbon from cycling through the EDEMP pathway and generating pyruvate for growth rather than phosphoenolpyruvate (PEP) to enter the shikimate pathway for product formation, *pgi-1* was deleted in a background strain where *pgi-2*

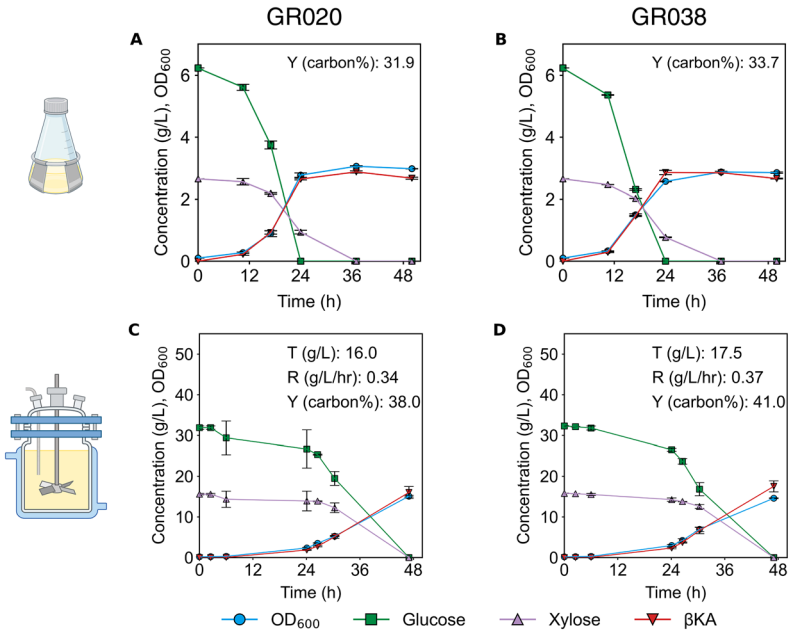

Fig. 2 Production of βKA from glucose and xylose by engineered *P. putida* KT2440 in shake flasks and bioreactors. Profiles are shown for glucose and xylose concentrations, growth (OD_{600}), and βKA production for strains (A and C) GR020 and (B and D) GR038, grown in either (A and B) shake flasks or (C and D) bioreactors operated in batch mode. Shake flask cultivations are displayed as the average of 3 biological replicates (n = 3) with error bars representing the standard deviation (σ). Bioreactor cultivations are displayed as the average of biological duplicates (n = 2) with error bars representing the range. Titer (T), rate (R), and yield (Y) metrics overlayed on graphs were calculated from final timepoints, with carbon% indicating C-mol yield. Created with BioRender.com.

was already absent, preventing the isomerization of fructose-6-phosphate to glucose-6-phosphate (Fig. 1). Deletion of *pgi-1* from GR020 generated GR023. No significant differences in growth or product formation were observed between strains GR023 and GR020 during growth on glucose (Fig. S1). However, when grown on a combination of glucose and xylose, growth of GR023 lagged by an additional 12 h (Fig. 2A and Fig. S2B). These results may indicate an imbalance in redox cofactors within primary metabolism during co-utilization of glucose and xylose when the EDEMP cycle is disrupted by the total abolition of PGI (glucose-6-phosphate isomerase) activity.

Deletions of *lvaE* and *gacS* and restoration of *pgi-1* enhance growth rate on mixed sugars

Under acidic conditions (pH < 7), βKA can undergo spontaneous non-enzymatic decarboxylation to levulinic acid, a compound that can be metabolized by *P. putida* through CoA-thioester intermediates followed by β-oxidation to acetyl-CoA for growth.[43] To avoid potential reuptake of carbon accumulated as βKA and allow accurate yield calculations from substrate to product, the gene responsible for the first step in levulinic acid catabolism (*lvaE*) was knocked out in GR023 to make strain GR029. Deletion of *lvaE* does not prevent the pH-dependent degradation of βKA to levulinic acid but may avert the reuptake of this carbon for growth. Previous work indicates that deletion of *lvaE* in a *P. putida* strain engineered for production of βKA from aromatics does not impact growth or improve product formation under the conditions evaluated;[14] in a strain engineered for production of levulinic acid from glucose, which proceeds through βKA, deletion of *lvaE* increased product formation by 80% in shake flasks.[44] Comparison of strains GR023 and GR029 revealed that deletion of *lvaE* did not impact growth or production metrics during growth on glucose, but surprisingly growth was improved (decreased lag and increased growth rate) relative to GR023 during growth on combined glucose and xylose (Fig. S1 and S2). Growth of GR029 still lagged relative to GR020 (Fig. 2A and Fig. S2C).

Adaptive laboratory evolution in muconic acid production strains previously revealed that deletion of *gacS*, part of a two-component (*gacAS*) signal transduction system, can improve product formation.[27,45] *gacAS* acts as a global regulatory system, controlling expression of a wide variety of genes and manifesting in myriad physiological responses (*e.g.*, motility, biofilm formation, secretory systems)[46]. Due to similarities between the muconic acid and βKA production pathways, we hypothesized that deletion of *gacS* would also improve βKA production strains. Deletion of *gacS* in strain GR029 yielded GR032. In plate-reader and shake-flask experiments, deletion of *gacS* did not impact growth or product formation during cultivation on glucose or on a mixture of glucose and xylose, relative to strain GR029 (Fig. S1 and S2).

While previous work has shown that muconic acid and βKA production from glucose are improved by the deletion of both *pgi* homologs (*pgi-1* and *pgi-2*),[5,6,45] we previously postulated

that the presence of *pgi-1* improves maximum theoretical yield when xylose is being co-utilized through the PPP.[24] Therefore, we restored *pgi-1* in the background without *gacS* (GR032) to yield GR038; restoration of *pgi-1* restored the growth phenotype of GR020 on glucose and xylose, confirming our hypothesis that PGI activity can improve growth when both sugars are present. In shake flask cultivations, GR038 performed similarly to GR020, producing 2.9 ± 0.07 g L^{-1} βKA from 6.2 g L^{-1} glucose and 2.6 g L^{-1} xylose in 24 h (Fig. 2B).

Evaluating βKA production by GR020 and GR038 in bioreactors in batch mode

While no differences were observed in strains GR020 and GR038 in shake flask experiments (Fig. 2A and B), prior work indicates that performance differences resulting from deletion of *gacS* may be evident in bioreactor cultivations.[27,47] To this end, these strains were grown in batch mode in 0.5-L bioreactors containing 30 g L^{-1} of glucose and 15 g L^{-1} of xylose. Sugars were depleted at 48 h by both strains, but production metrics were slightly higher in GR038 (17.5 ± 1.36 g L^{-1}, 0.37 ± 0.03 g L^{-1} h^{-1}, 0.41 ± 0.03 C-mol yield) compared to GR020 (16.0 ± 1.46 g L^{-1}, 0.34 ± 0.03 g L^{-1} h^{-1}, 0.38 ± 0.03 C-mol yield) (Fig. 2C and D).

βKA production in bioreactors operated in fed-batch mode

To improve βKA production metrics, GR038 was subsequently grown in 10-L bioreactors in fed-batch mode, where feed rate was manually adjusted based on glucose and xylose consumption rates. After the growth lag phase (Fig. 3B), we observed rapid sugar consumption (maximum utilization rate: 3.1 g L^{-1} h^{-1}) and βKA production from 12 h onwards in strain GR038 (Fig. S3). The βKA titer, productivity, and yield achieved at 96 h were 65.8 g L^{-1}, 0.69 g L^{-1} h^{-1}, and 0.52 C-mol/C-mol, respectively.

Adsorptive ISPR improves βKA production by GR038

Often, product inhibition is the limiting factor for enhancing performance metrics. Thus, we coupled ISPR to bioreactor cultivations to mitigate potential product inhibition.[30–36] Prior to integration, we screened three anion-exchange resins for their βKA adsorption capacity using packed-bed columns and the single frontal method[48] (Fig. S4). Amberlite IRA-910, a type II strong anion-exchange resin, was selected based on its high adsorption capacity for βKA among the screened resins (Table 2).

Reuse and regeneration of Amberlite IRA-910 was validated by processing GR038 cultivation broth over 20 bind-and-elute cycles (Fig. S5). The results indicate that the adsorption capacity of IRA-910 remained constant between cycles and that βKA was fully recovered from the resin during elution. Subsequently, Aspen Chromatography (Aspen Technology, Inc.) was used to model the bind-and-elute cycle (Fig. S5A) and to predict column behavior at different βKA concentrations (Fig. S5B), flow rates, and column lengths. Within Aspen Chromatography, we also modeled competitive adsorption to account for binding of media components including chloride, phosphate, sulfate, and hydroxide ions to show the reduced purity of βKA due to the competing anions, which are also removed from the resin during an elution cycle. The combined experimental and Aspen model results were ultimately used to set the column size, cycle duration, and flow rate for the two-column adsorptive ISPR system.

The adsorptive ISPR system was then connected to a 3-L bioreactor (see configuration in Fig. 3A). Following the flow path from the exit of the bioreactor, the bioreactor broth was first subjected to microfiltration *via* a rotating ceramic disc (RCD) filter (0.2 μm pore size) to prevent cells from fouling the downstream adsorption columns.[49,50] An RCD is a dynamic filtration device that uses rotation to generate a high shear rate (10^4 to 10^5 s^{-1}) at the membrane surface to increase membrane flux and reduce fouling.[51] The permeate from the RCD was directed to two packed-bed columns containing the IRA-910 anion-exchange resin. Adsorption of βKA on the IRA-910 resin releases NH_4OH into the 'media recycle' stream as the resin releases its counterion, a hydroxide ion, and the βKA releases its ammonium ion. Post-adsorption, the βKA-depleted broth was sent back to the bioreactor as recycled production medium or collected in a separate vessel to balance the sugar-feeding volume additions. During desorption, 0.5 M NaOH was used to elute βKA from the column and regenerate the resin with hydroxide ions. A detailed description of the equipment and settings used for alternating column operation is given in the Materials and Methods section.

The cultivation of GR038 was conducted in fed-batch mode, with feeding rates adjusted manually based on sugar utilization rates (Fig. S3). The cultivation broth was introduced into the external loops at 45 h to initiate βKA removal, indicated by a vertical dashed line in Fig. 3B and C, with adsorption and desorption cycles (102 cycles) performed over the remainder of the cultivation. βKA reached an effective titer of 92.0 g L^{-1} with a productivity of 0.83 g L^{-1} h^{-1}, representing a substantial improvement over the fed-batch case without ISPR, and implying mitigation of product inhibition by using ISPR. The volumetric titer based on cultivation volume is compared to the fed-batch results (without ISPR) in Fig. 3A. During the ISPR operation, we observed that βKA accumulation in the bioreactor was reduced compared to the previous fed-batch case (Fig. S3). Total βKA accumulation was split between the bioreactor and the adsorption collection vessel over the course of cultivation, as shown in Fig. 3C, with 38% of the total βKA removed by ISPR at 111 h, the time point when productivity began to decrease substantially.

Downstream processing

The use of βKA as a monomer necessitates an end-product with polymer-grade purity. Here, we compare the purity of βKA obtained from a previously developed post-processing approach[6] with the purity of βKA obtained post adsorptive ISPR. Each approach uses acidification, liquid–liquid extraction (LLE), and precipitation. Differently, the previously developed post-cultivation processing method uses sequential batch processing steps, including filtration, activated carbon treatment, acidification, LLE, and precipitation.[6] Application of

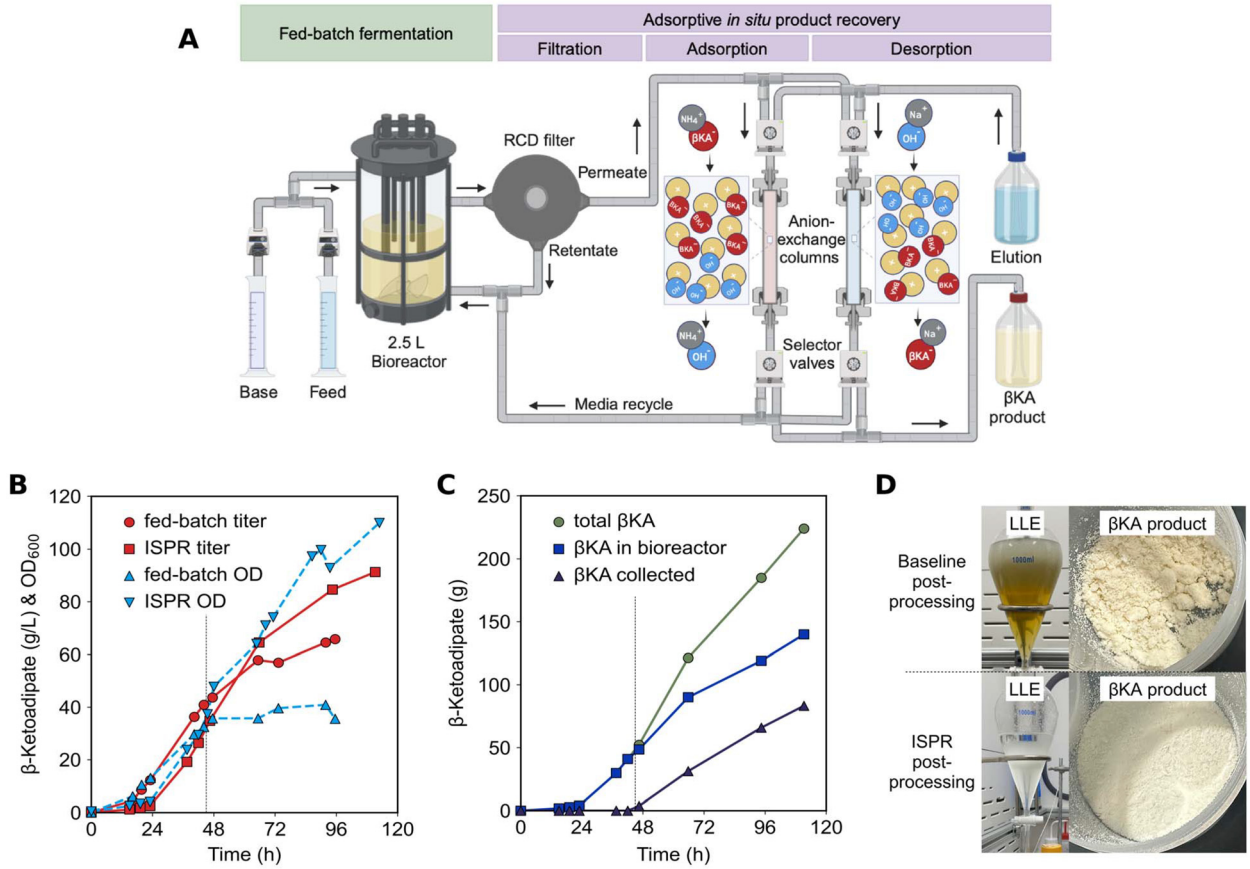

Fig. 3 Adsorptive ISPR schematic and bioreactor profiles in cultivations conducted in fed-batch mode with or without ISPR integration. (A) The schematic shows the bioreactor setup coupled to the adsorptive ISPR unit operations. The flow path from the bioreactor first proceeds through a rotating ceramic disc (RCD) microfiltration unit and then to anion-exchange columns. The adsorption columns alternated between βKA adsorption and desorption to recover βKA from the columns. During adsorption, at each anion-exchange site, the βKA anion replaces a bound hydroxide ion. During desorption *via* 0.5 M NaOH, the bound βKA anion is recovered as sodium βKA and hydroxide binds to the resin. (B) Comparison of cultivations with and without adsorptive ISPR, showing OD_{600} and βKA titer. ISPR operation began at 45 h of the adsorptive ISPR cultivation, as indicated by the vertical dashed line. During ISPR, the concentration of βKA in the bioreactor remained lower than the βKA concentration in the bioreactor during the fed-batch cultivation without adsorptive ISPR (Fig. S3). (C) βKA accumulation within the adsorptive ISPR system was split between βKA in the bioreactor and βKA in the collection vessel after elution. The total amount (combined ISPR collection and bioreactor) of βKA within the system reached 224.2 g at the end of the cultivation. (D) βKA collected during ISPR operation was subjected to post-processing. The left images show the reduced coloration and emulsion formation during ethyl acetate extraction prior to solvent evaporation for the adsorptive ISPR compared to the baseline post-processing method,[6] and the right images show the final, dried product. Panel A was created with BioRender.com.

Table 2 βKA capacity of anion-exchange resins

Resin ID	Copolymer (matrix)	Functional group (type)	Capacity (g βKA/mL of bed volume)
Amberlyst A26	Styrene-divinylbenzene (macroporous)	Trimethylammonium (type I)	0.78
Amberlite IRN-78	Styrene-divinylbenzene (gel)	Trimethylammonium (type I)	0.90
Amberlite IRA-910	Styrene-divinylbenzene (macroporous)	Dimethylethanol-ammonium (type II)	0.92

ISPR resulted in substantial improvement in βKA purity (88.3 wt% to 99.0 wt%) and reduced concentration of several elements, some of which could serve as polymerization inhibitors, in the final product (elements present in the M9 medium include Fe, Mg, P, and K) (Fig. S6). In addition to a reduction in key elements, the ISPR sample showed substantially less water content compared to the baseline sample (5.0 wt% *vs.* 0.9 wt%). Lastly, the presence of the decarboxylation product levulinic acid, as well as inorganic content, was quantified by HPLC (Fig. S7) and TGA (Table S2) with the ISPR sample showing substantially less impurities and lower levulinic acid content compared to the baseline sample.

Discussion and conclusions

βKA is an alternative to petroleum-derived adipic acid and castor oil-derived sebacic acid in performance-advantaged nylons.[6] The current study provides a substantial improvement on βKA production using engineered strains of *P. putida*. Prior to this work, production of βKA from sugars was achieved with *P. putida* SN301, which was unable to utilize xylose. By employing rational engineering approaches for improved pathway flux and utilization of xylose as an additional carbon source, we doubled the titer in bioreactors in fed-batch mode and improved productivity by reducing the growth lag phase in GR038 relative to SN301 by 20 h. Implementation of adsorptive ISPR further improved effective titer and productivity of βKA (92.0 g L^{-1} and 0.83 g L^{-1} h^{-1}, respectively), and post-processing of the adsorptive ISPR-collected βKA resulted in increased purity compared to results obtained in our previous work (99.0 wt% *vs.* 88.3 wt%).[6] Together, these improvements represent a more-than three-fold improvement in effective titer and almost ten-fold improvement in productivity, as well as the development of a continuous separations method to isolate βKA at purity approaching that needed for polymerization.

The metrics achieved for βKA production in this work from fed-batch cultivation (without ISPR) roughly doubled the titer and quadrupled the rate achieved for muconic acid with the parent strain LC224 (65.8 g L^{-1} *vs.* 33.7 g L^{-1}, 0.69 g L^{-1} h^{-1} *vs.* 0.18 g L^{-1} h^{-1}).[24] As primary metabolism and direction of carbon through the shikimate pathway are identical between βKA and muconic acid production strains, carbon flow from the last common intermediate, PCA, to the final product is likely faster in βKA strains; differences in product formation between these pathways could result from both kinetic and thermodynamic driving forces. While the pathway from PCA to muconic acid is heterologous, the PCA-to-βKA pathway exists in native *P. putida* metabolism. Both pathways rely on a ring-opening dioxygenase, either CatA or PcaHG, and these reactions unsurprisingly provide, by far, the largest thermodynamic driving force for the pathways (Fig. 4). The placement of this ring-opening reaction, a committed step, as the first reaction between PCA and βKA might increase flux to the final product. Although more reactions are involved, βKA synthesis exhibits a more thermodynamically favorable free energy change (−372 kJ mol^{-1}) relative to the muconic acid pathway (−323 kJ mol^{-1}) (Fig. 4).

Regarding kinetic differences, the first step from PCA to muconic acid is the decarboxylation to catechol by AroY. This heterologously-expressed enzyme is hypothesized to be a bottleneck in muconic acid production due to poor kinetics, which result in accumulation of PCA and catechol.[52,53] Availability of prenylated-FMN cofactor required for AroY activity may be a limiting factor. Similarly, cleavage of catechol by CatA has been proposed as a bottleneck, a hypothesis supported by improved muconic acid production in strains overexpressing CatA or containing mutated CatA variants.[54,55] Accumulation of PCA or intermediate metabolites in the βKA pathway has not been observed in GR038. Together, these factors likely explain why βKA production outpaces muconic acid production in strains GR038 and LC224, respectively.

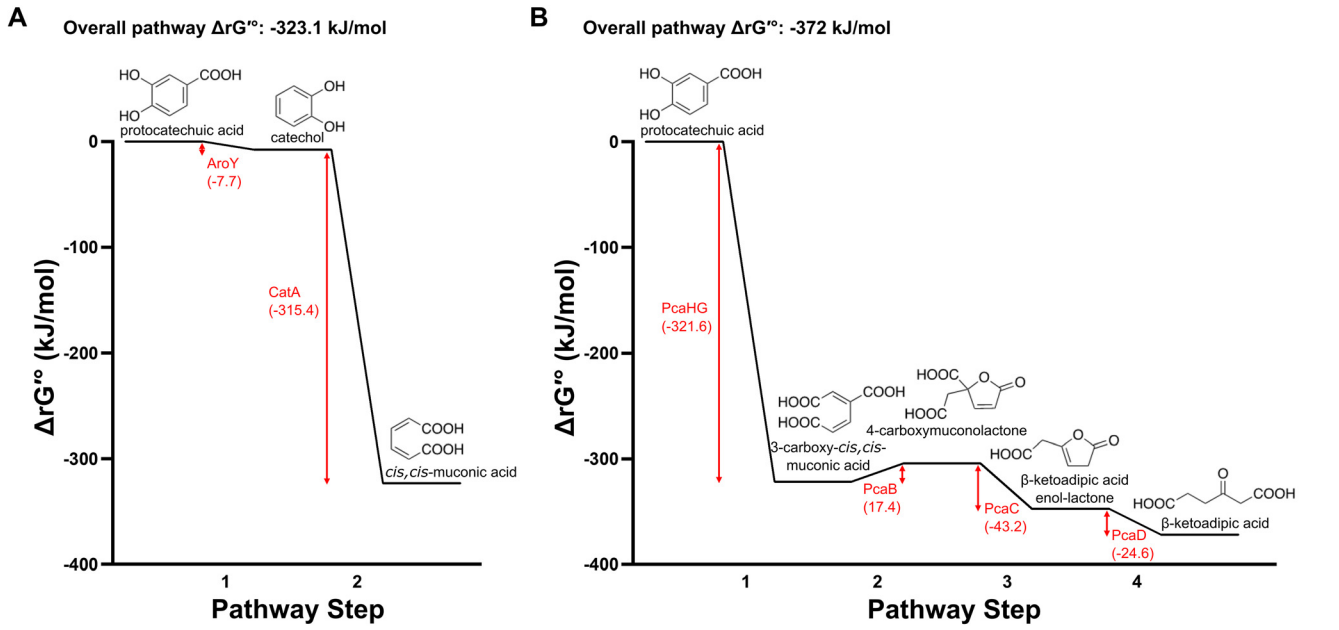

Fig. 4 Thermodynamic comparison of pathways from PCA to muconic acid and βKA. Both (A) muconic acid and (B) βKA are C6 diacids metabolically downstream of PCA. The change in free energy associated with each reaction is shown in red. While the pathway from PCA to muconic acid is engineered, the βKA pathway exists in native *P. putida* metabolism. Changes in free energy, $\Delta_r G'°$, were estimated with eQuilibrator 3.0, which utilizes a group contribution method (component contribution).[56] The cofactor prenylated-FMN is abbreviated as prFMN. A full list of abbreviations for gene names is provided in Table S1.

Product formation was also improved by using a continuous strong ion adsorptive ISPR process to relieve product inhibition. One of the challenges overcome in this study was in achieving continuous, rather than intermittent, ion exchange. Ion exchange is challenged by the release of hydroxide ions during adsorption that may shift the pH of the bioreactor, leading to increased dosing of acid and salt accumulation in the bioreactor if the rate of adsorption is too rapid. Accordingly, the pH must be regulated if the adsorption system is oversized, as a previous study used a pH controller to turn on and off the recycle adsorption loop to control pH during adsorptive ISPR for lactic acid production.[57] Several other reports employed intermittent adsorptive ISPR with one or two columns to reduce pH impacts.[31,34,35,38] Here, we achieved uninterrupted adsorptive ISPR and stable pH by scaling two small (7.3 mL) columns that alternated through the adsorption and desorption cycle with a rapid cycle time (30 min) to match the adsorption rate to the strain productivity. This twin-column method also allowed for continuous adsorption activity during the entire ISPR demonstration and continuous cycling between columns. Further system improvements could focus on the recovery of the βKA remaining in the bioreactor at the end of the run, which was in sufficient quantity (62 wt% of total accumulated in system, Fig. 3).

Adsorptive ISPR also enabled us to reduce the number of purification steps and chemical footprint.[39,58] Namely, adsorptive ISPR enabled the elimination of activated carbon treatment, reduced emulsion formation during LLE, and increased product purity from 88.3 wt% to 99.0 wt%. (Fig. S5 and S6). TGA and FTIR revealed that the baseline sample had a lower CO_2-to-levulinic acid molar ratio (0.9 : 1) than the ISPR sample (1.2 : 1). A molar ratio less than 1 : 1 may indicate the formation and presence of levulinic acid in the final post-processing isolate (a CO_2 : levulinic acid molar ratio of 1 : 1 indicates pure βKA as 1 mol of βKA decarboxylates into 1 mol of CO_2 and 1 mol of levulinic acid). Acid hydrolysis is accelerated under acidic conditions and the presence of 5 wt% water (pH < 3) in the baseline sample (compared to 0.9 wt% in the ISPR sample) may have caused significant decarboxylation before the samples were frozen. The higher water content within the baseline sample was promoted by the observed emulsion formation during LLE. We did not observe emulsion formation in the ISPR LLE step. Images from the last two purification steps (LLE and precipitation) for each case are shown in Fig. 3D to highlight the visual differences during LLE. However, we did observe by ICP-OES a small increase in sodium and sulfur content in the ISPR product compared to the baseline sample. This is because sodium sulfate was used to dry the samples and the increase is attributed to incomplete washing prior to storage. While our purification reached 99.0 wt% βKA purity, this is slightly lower than the purity reported for muconic acid (99.8%) separated from *P. putida*.[54] The slight decrease in reported purity is likely due to the residual water in the isolate.

Process modeling and techno-economic analysis performed as part of our previous work estimated a minimum selling price of $1.94 per kg when producing βKA from glucose, assuming production metrics of 90 g L^{-1}, 1 g L^{-1} h^{-1}, and 0.40 C-mol yield, which are comparable to the metrics achieved in this study.[6] Consequently, the previous analysis suggests our process could hold promise as a means of producing βKA at near cost parity with the incumbent petroleum-derived adipic acid ($1.00–2.50 per kg). Likewise, that analysis also showed reduced sensitivity of the βKA minimum selling price above 60 g L^{-1} and 40% yield, indicating that the metrics achieved here are promising for further scale-up.

Materials and methods

Strain and plasmid construction

Strains and plasmids were constructed using the methods from Ling *et al.*[24] Plasmids were generated with NEBuilder HiFi DNA Assembly Master Mix (New England Biolabs), according to the recommended protocol from the manufacturer. Linear fragments for assembly were generated by PCR with Q5 Hot Start High-Fidelity 2× Master Mix (New England Biolabs). To eliminate plasmids of cellular origin and prevent carryover of the template plasmid, PCR reactions amplifying the vector backbone were digested with DpnI. Prior to assembly, fragments were purified with the DNA Clean and Concentrator Kit (Zymo Research), following the instructions from the supplier. After assembly, 2 μL of the reaction mixture was transformed into 5-alpha F′I^q chemically competent *E. coli* (New England Biolabs) by heat-shock (30 s at 42 °C) and outgrowth in SOC medium (Sigma-Aldrich) was performed for 1 h at 37 °C, 250 rpm. Transformants were selected overnight on LB agar (Lennox) plates containing 50 μg mL^{-1} kanamycin (Sigma-Aldrich). Correct clones were identified by PCR screening with Q5 Hot Start High-Fidelity 2× Master Mix (New England Biolabs) and sequence verified by whole-plasmid nanopore sequencing (Plasmidsaurus). Plasmid DNA was isolated with the ZymoPURE Plasmid Miniprep kit (Zymo Research).

Genetic manipulation of *P. putida* was accomplished as described by Johnson and Beckham.[59] Strains to be transformed were inoculated from glycerol stocks into 24 mL culture tubes containing 5 mL of LB (Miller) medium and incubated overnight at 30 °C with agitation at 225 rpm. Flasks containing 10 mL of LB medium were inoculated from overnight cultures to an OD_{600} of 0.2 and grown to an OD_{600} of ~0.5–0.6. Cells were harvested by centrifugation in 50 mL falcon tubes at 4200*g* and washed by resuspending in 1 volume ice-cold 300 mM sucrose. Cell pellets were washed twice more with $\frac{1}{2}$ volume ice-cold 300 mM sucrose, and finally resuspended in 1/100 volume ice-cold 300 mM sucrose.[60] Electroporation was conducted in 1 mm cuvettes using a Gene Pulser Xcell (Bio-Rad) set to 1.6 kV, 200 Ω, and 25 μF. After outgrowth for 1–2 h in 1 mL SOC medium (Sigma-Aldrich) at 30 °C with agitation at 225 rpm, integration of plasmids into the genome was selected by growth on LB agar (Lennox) plates containing 50 μg mL^{-1} kanamycin. Transformants were restreaked twice on kanamycin plates before counterselection on YT agar plates supplemented with 15% sucrose.

Transformants were initially identified by colony PCR and confirmed with Sanger sequencing (GeneWiz).

Plasmids utilized in this work are described in Table S3. The confirmation of genetic alterations was verified by genome sequencing each successive change at the modified locus, and then whole genome sequencing of the final strain. Primers utilized for genetic confirmation were synthesized by Integrated DNA Technologies (IDT) and are described in Table S4. Whole-genome sequence data for strain GR038 is available through the Sequence Read Archive (SRA) under BioProject ID number PRJNA1171460.

Plate reader growth

Cultivations were prepared as described in Amendola *et al.*[61] Pre-cultures were inoculated from glycerol stocks into 5 mL of LB (Miller) medium in 24 mL culture tubes and incubated overnight at 30 °C with shaking at 225 rpm. Cells were pelleted by centrifugation at 3000*g* and resuspended in 1 mL of 1× M9 salts. Cells were pelleted and washed again, OD_{600} was measured, and each strain was diluted to an OD_{600} of 0.1 in M9 minimal medium supplemented with 5.4 g L^{-1} glucose. Microtiter plates were inoculated with 200 μL of each strain in triplicate wells. Uninoculated medium was included as a negative control. Growth was conducted at 30 °C in a Bioscreen C Pro (Growth Curves USA) with continuous orbital shaking set to maximum amplitude.

Shake flask cultivations

Pre-cultures were inoculated from glycerol stocks into 24 mL culture tubes containing 5 mL of LB (Miller) medium and incubated overnight at 30 °C with agitation at 225 rpm. Seed cultures of 10 mL LB (Miller) medium in metal-capped 125 mL baffled flasks were inoculated from overnight pre-cultures at an initial OD_{600} of 0.2 and incubated under the same growth conditions for 4 h or until OD_{600} reached ~2. Seed cultures were harvested by centrifugation at 3000*g* for 5 min and washed twice by resuspending in 1× M9 salts (6.78 g L^{-1} Na_2HPO_4, 3 g L^{-1} KH_2PO_4, 0.5 g L^{-1} NaCl, 1 g L^{-1} NH_4Cl) before inoculation of experimental cultures to an OD_{600} of 0.1. Shake flask cultivations were performed in biological triplicates in metal-capped 125 mL baffled flasks containing an initial culture volume of 30 mL, incubated at 30 °C with shaking at 225 rpm, unless otherwise noted. Growth was conducted in M9 medium consisting of 6.78 g L^{-1} Na_2HPO_4, 3 g L^{-1} KH_2PO_4, 0.5 g L^{-1} NaCl, 1 g L^{-1} NH_4Cl, 2 mM $MgSO_4$, 100 μM $CaCl_2$, and 18 μM $FeSO_4$, and supplemented with 6.2 g L^{-1} glucose (Sigma-Aldrich) and 2.6 g L^{-1} xylose (Sigma-Aldrich). Monosaccharide concentrations were chosen to mimic the 2 : 1 molar ratio of glucose : xylose typically present in hydrolysates of corn stover.[62] For growth measurements and HPLC analysis, 1 mL samples were collected at indicated time points. After OD_{600} measurements, samples were centrifuged at >20 000*g* to remove cells and supernatant was passed through a 0.2 μm filter before storing at −20 °C for downstream analysis.

Bioreactor cultivations in batch and fed-batch mode without ISPR

Bioreactor cultivations for strain evaluation in batch mode were conducted in 0.5 L vessels (250 mL initial volume) using the BioStat-Q Plus system (Sartorius Stedim Biotech). Conditions in the bioreactors were controlled at 30 °C and at pH 7 by addition of 7 N NH_4OH, and air was sparged at 1 vvm. Bioreactor cultivations were initiated with DO levels of 100%, with the agitation rate set at 350 rpm. When the DO level reached 30%, it was maintained by automatically adjusting the agitation. The seed cultures were prepared in 250 mL baffled flasks containing 50 mL LB (Miller) inoculated with the strains from glycerol stocks. The seed cultures were prepared in duplicate and incubated at 30 °C and 225 rpm for 16 h. Each replicate of the seed was used to inoculate independent bioreactors at an initial OD_{600} of 0.2. An appropriate volume of the seed was centrifuged (5000*g*, 10 min), the supernatant was discarded, and the cells were resuspended in 5 mL of modified M9 medium (13.56 g L^{-1} Na_2HPO_4, 6 g L^{-1} KH_2PO_4, 2 g L^{-1} $(NH_4)_2SO_4$, 1 g L^{-1} NaCl, 2 mM $MgSO_4$, 100 μM $CaCl_2$ and 36 μM $FeSO_4$).

Batch mode bioreactor cultivations were conducted using a 250 mL batch medium consisting of modified M9 supplemented with 50 g L^{-1} of sugars (33 g L^{-1} glucose and 17 g L^{-1} xylose) to imitate the molar ratio of glucose to xylose in hydrolysates of corn stover.[62] Cultivation was terminated once all sugars were consumed, as confirmed by an offline sugar analyzer (YSI 7100 Multiparameter Bioanalytical System, Xylem Analytics).

Fed-batch cultivations were conducted in a 10-L Applikon bioreactor. The cultivation began with a batch phase wherein the initial medium consisted of 5500× mL modified M9 and 15 g L^{-1} of sugars (10 g L^{-1} glucose and 5 g L^{-1} xylose) and 10% (v/v) of an LB solution (25 g L^{-1}). For fed-batch cultivations, the first seed culture was used to inoculate a second seed in 1000 mL baffled shake flasks containing 550 mL LB broth at an initial OD_{600} of 0.2. After approximately 5 h, the second seed reached an OD_{600} of 2.0 and the whole seed was used to inoculate the bioreactor. We maintained a total sugar concentration of ~5–20 g L^{-1} in bioreactors (adjusted manually) by continually feeding concentrated sugars as dictated by consumption rates. The feeding medium contained 453 g L^{-1} total sugars (300 g L^{-1} glucose and 153 g L^{-1} xylose, 2 : 1 molar ratio). Cultivation was terminated once the bioreactor reached its maximum volume capacity (10 L).

Bioreactor cultivations in fed-batch mode with ISPR

Adsorptive ISPR fed-batch cultivation was performed in a 3-L Applikon bioreactor. Initially, the bioreactor was not coupled to the ISPR unit to avoid column adsorption of essential media components before sufficient growth could occur. The cultivation began with a batch phase wherein the initial medium consisted of 1200 mL modified M9 containing 25 g L^{-1} total sugars (17 g L^{-1} glucose and 8 g L^{-1} xylose, 2 : 1 molar ratio) and 10% (v/v) of an LB solution (25 g L^{-1}). Here the second seed was prepared in a 500 mL baffled shake

flask containing 120 mL LB broth and was also grown for approximately 5 h, after which the entire volume was utilized to inoculate the bioreactor. Total sugar concentration of ~5–20 g L^{-1} was maintained in the bioreactor (adjusted manually) by continually feeding concentrated sugars as dictated by consumption rates. The adsorptive ISPR unit was coupled to the bioreactor at 45 h when sufficient cell growth had been achieved (OD_{600} of 37.33). Starting at 68 h we removed fermentation broth at a rate of 16 mL h^{-1} to avoid overflow by diverting flow from the permeate stream of the RCD filter to a product diversion reservoir. Cultivation was terminated due to excessive foaming at 112 h as a result of high cell densities and agitation rates.

Quantification of sugars

Glucose and xylose were quantified as described in Alt *et al.*[63] Briefly, samples and standards were analyzed by high-performance liquid chromatography with a refractive index detector (HPLC-RID) using a Bio-Rad Aminex HPX-87H ion-exclusion column to provide chromatographic separation with an aqueous sulfuric acid mobile phase.

Quantification of βKA

βKA was analyzed as previously detailed in Rorrer *et al.*[6] In short, βKA decarboxylates abiotically, therefore, to enable the most accurate quantification of the product, all βKA was hydrolyzed to levulinic acid using sulfuric acid and heat. βKA was subsequently quantified as levulinic acid. Samples and standards were analyzed using identical HPLC conditions for sugar analysis above.

Yield and rate calculations

C-mol yields (%carbon) were calculated as C-mol product (βKA) produced per C-mol sugar substrate consumed (C-mol glucose plus C-mol xylose); mol substrates consumed and product generated were converted to single carbon equivalents for each compound by multiplying the concentration of each substrate consumed and product generated by the number of carbon atoms in the molecule. Sugar substrates in cultivation media were measured at all sampling points throughout growth, with substrate consumption calculated as the difference between final and initial substrate present. Final or maximal βKA concentrations (as reported) were used to calculate yield based on the corresponding sugar consumption measurements. Production rates (g L^{-1} h^{-1}) were calculated as product concentration per cultivation time. Effective titer (g L^{-1}) for ISPR was calculated as the total system βKA (g) normalized to the bioreactor volume (L).

Adsorption capacity *via* the single frontal method

Strong-base anion-exchange resins (DuPont) Amberlite IRA-910 Cl, Amberlyst A26 OH, and Amberlite IRN78 OH were cleaned by sonication in ultra-pure water (UPW), obtained through a Milli-Q® system (Fisher Technologies), and rinsed with UPW through a sieve. Columns were packed into Diba Omnifit™ EZ chromatography columns with a bed volume of 0.5 mL (inner diameter 0.66 cm, length 1.50 cm), using the ÄKTA Pure (Cytiva). The column containing Amberlite IRA-910 was then washed with 2 M NaOH at 2 mL min^{-1} for three bed volumes to convert the ion from Cl to OH. Purified βKA (from post-processing) was used to make a 0.1 M βKA solution to perform a single frontal test[48] on all three packed columns. βKA adsorption was monitored using UV adsorption at 255 nm (Fig. S5C) until equilibrium was reached. The adsorption was calculated using the anion-exchange model (eqn (1)):

$$\text{AEC} = (\text{amount of } \beta\text{KA absorbed/column bed volume}). \quad (1)$$

The center of mass of the frontal curve was used to determine the amount of βKA absorbed per bed volume for each resin (Table 2).

Preliminary column tests

Broth from a single-batch βKA cultivation with a titer of 65 g L^{-1} was used to perform adsorption and desorption cycles on 7.3 mL columns packed with IRA-910 resin. The cultivation broth was prepared by microfiltration (0.2 μm) using a ceramic membrane RCD (Andritz DCF 152/S) to remove any remaining cells. βKA broth was loaded onto the packed column until the UV 255 mAU signal on the column flow-through stabilized, indicating that the column was equilibrated with βKA. Two bed volumes of UPW were flushed through the column to wash unbound acids, then 0.5 M NaOH was used to elute the βKA. This method was replicated on the same column for 20 cycles to confirm consistent recovery (Fig. S5). Samples from all stages were collected and βKA concentration was determined using HPLC.[6]

Aspen chromatography

Aspen Chromatography was used to simulate a batch mode fixed-bed single column system with one feed stream and one effluent. Cultivation broth component concentrations and column dimensions (Table S5) were used to model the adsorption behavior of βKA, which can be used to optimize column sizing and flow rates for ISPR implementation. Modeling was first validated against the single cycle runs, then column sizing, flow rates, and cycle times were adjusted until the rate of removal matched the rate of production based on the single-batch cultivation (Fig. S5).

Adsorptive ISPR

The adsorptive ISPR system consisted of automated controls to continuously or intermittently separate βKA using one RCD filter and two IRA-910 adsorption columns (7.3 mL). Pumps were primed with water *via* a manual syringe and integration was initiated 45 h into the cultivation. The broth was initially filtered by the RCD at 4–5 psig while the disc rotated at 1000 rpm. The retentate was returned to the bioreactor while the permeate was pumped into a collection vessel. The permeate collection vessel used three level sensors to initiate loading of filtered broth onto a column once the volume of permeate was adequate for a load cycle. These sensors turned off the load

cycle if the volume decreased past the required volume. Filtered broth was loaded onto one column at 2 mL min^{-1} for 30 minutes and effluent was returned to the bioreactor. UPW was then used to wash the column at 5 mL min^{-1} for 3 minutes and collected in a wash reservoir. βKA was eluted off the column and collected for downstream processing using 0.5 M NaOH at 5 mL min^{-1} for 5 minutes. Cycles concluded with a UPW regeneration at 5 mL min^{-1} for 7 minutes to remove NaOH from the column.

Downstream processing

A previously reported post-processing separation βKA method[6] was completed in parallel to the separations post ISPR to isolate βKA. Briefly, the previously reported method included treating filtered broth (65 g L^{-1} βKA) with 8 g L^{-1} activated carbon and stirring for 2 h.[6] Post activated carbon, the previously reported method and post ISPR separations included an acidification step where 500 mL of broth was adjusted to a pH of 2 using sulfuric acid (Sigma-Aldrich, ACS reagent). Two stages of LLE were used with equal volume of acidified broth to ethyl acetate (Sigma-Aldrich, ACS reagent) during each step to isolate βKA in the ethyl acetate. Excess sodium sulfate (~8 g L^{-1}) was added to dry the product. Vacuum distillation was conducted using a Rotovapor R-300 (BUCHI) with parameters set at a water bath temperature of 30 °C, 150 rpm, and 120 mbar. The remaining product was washed with anhydrous chloroform (Sigma-Aldrich) to remove any levulinic acid formed due to decarboxylation during processing.

βKA purity measurements

FTIR-TGA evolved gas analysis (EGA) was conducted to analyze the composition of the synthesized βKA powder from the single-batch and βKA from ISPR product samples. Approximately 7–10 mg of sample were loaded into a tared 110 μL platinum TGA pan. The pan was then placed into a Discovery SDT 650 (TA Instruments) connected to a Spectrum 3 FT-IR (PerkinElmer) spectrometer equipped with a TL 8000 Balanced Flow FT-IR EGA system. A TGA-IR Interface TL 8000 (PerkinElmer) was used to set the temperature of the adapter, cell, and TL-TGA of the EGA system to 270 °C and the flow to 70 mL min^{-1}. A background spectrum was performed on the Spectrum 3 before each sample was run with a resolution of 4 cm^{-1} and an accumulation set to 64 scans. The sample pan was then heated under nitrogen (100 mL min^{-1}) from ambient temperature to 240 °C at a ramp rate of 50 °C min^{-1}, where complete weight loss was observed (Fig. S6A).

A simultaneous experiment was conducted on the Spectrum 3 to analyze the evolved gas from the Discovery SDT 650 using a wavenumber range from 650–4000 cm^{-1}, a resolution of 4 cm^{-1}, and an accumulation set to 2 scans. Signals corresponding to CO_2 (2300–2400 cm^{-1}) and levulinic acid (1700 cm^{-1} and 3000–3500 cm^{-1}) were monitored to confirm the decarboxylation of βKA, which releases CO_2 and transforms into levulinic acid (Fig. S6B). The pan was cleaned after each run by running an isometric hold at 700 °C for 10 minutes. All TGA curves were analyzed using TA Instruments' Trios software while all FT-IR spectra were analyzed using PerkinElmer's Spectrum IR software. The percent weight loss at each event was calculated, and the expected percent weight loss based on the molecular weights of CO_2 and levulinic acid in βKA was used to determine purity.

ICP-OES

Inductively coupled plasma optical emission spectroscopy (ICP-OES) was used to analyze the elemental composition of both samples. The analysis was conducted using a Milestone – Ultrawave Single Reaction Chamber Microwave Digester and an Agilent 5110 ICP-OES. Prior to analysis, approximately 100 mg of each sample was weighed and digested in 4 mL of nitric acid. The digestion process involved ramping the temperature to 225 °C to ensure complete dissolution of the sample matrix. Subsequently, the digested samples were diluted to a final volume of 15 mL. A comprehensive quantitation of elements was performed, and emission intensities were measured at the respective wavelengths for each element of interest (Fig. S6C). The concentrations of elements were reported in parts per million (ppm), calculated based on the calibration curves from 0–20 ppm obtained from standard solutions.

Data statistics

For individual figures, data statistics are noted in figure captions. Generally, shake flask experiments were conducted in biological triplicate (n = 3), with data shown as an average (mean) and error bars representing standard deviation (σ). For batch mode bioreactors, data is shown as the average (mean) of biological duplicates (n = 2) with error bars representing the range.

Author contributions

GTB, CWJ, and DS conceptualized and oversaw the project. GMR performed metabolic engineering. GMR and SCM performed microbial cultivations. SCM, LC, ARL, and POS performed the ISPR experiments. ARL, HC, and POS performed separations and post-processing. MAI and KJR performed metabolite analysis. GMR, LC, ARL, and POS generated data visualizations. GMR, ARL, POS, and GTB wrote the manuscript. GMR compiled author contributions. All authors discussed and commented on the final manuscript.

Conflicts of interest

There are no conflicts to declare.

Data availability

The numerical data supporting this article are contained in the SI, including the underlying experimental datasets (SI Excel 1).

SI containing Fig. S1–S7 and Tables S1–S5 is available. See DOI: https://doi.org/10.1039/d5gc01813g.

Acknowledgements

This work was authored in part by the National Renewable Energy Laboratory for the U.S. Department of Energy (DOE) under Contract No. DE-AC36-08GO28308. Funding was provided by the U.S. DOE Office of Energy Efficiency and Renewable Energy Bioenergy Technologies Office (BETO) for the Agile BioFoundry and the Bioprocessing Separations Consortium *via* contract no. DE-AC36-08GO28308. We thank Chen Ling for his work generating and supplying the parent strain, conceptual design for xylose utilization, and insightful discussions concerning the experimental approach. We thank Joel Miscall for conducting the ICP-OES analysis, Hannah Alt and Sean Woodworth for analytics, Manar Alherech for insights about quantifying βKA purity, and Gayle Bentley, Lisa Guay, and Sonia Hammache at DOE, Alissa Bleem, Caroline Amendola, Allison Yaguchi, and other members of the Agile BioFoundry and Separations Consortium for helpful discussions. The U.S. Government retains and the publisher, by accepting the article for publication, acknowledges that the U.S. Government retains a nonexclusive, paid-up, irrevocable, worldwide license to publish or reproduce the published form of this work, or allow others to do so, for U.S. Government purposes.

References

1 G. Fuchs, M. Boll and J. Heider, *Nat. Rev. Microbiol.*, 2011, **9**, 803–816.
2 E. M. Spence, H. T. Scott, L. Dumond, L. Calvo-Bado, S. di Monaco, J. J. Williamson, G. F. Persinoti, F. M. Squina and T. D. H. Bugg, *Appl. Environ. Microbiol.*, 2020, **86**, e01561–e01520.
3 R. J. M. Lubbers, A. Dilokpimol, P. A. Nousiainen, R. C. Cioc, J. Visser, P. C. A. Bruijnincx and R. P. de Vries, *Microb. Cell Fact.*, 2021, **20**, 151.
4 E. Kuatsjah, A. Schwartz, M. Zahn, K. Tornesakis, Z. A. Kellermyer, M. A. Ingraham, S. P. Woodworth, K. J. Ramirez, P. A. Cox, A. R. Pickford and D. Salvachúa, *Cell Rep.*, 2024, **43**, 115002.
5 C. W. Johnson, D. Salvachúa, N. A. Rorrer, B. A. Black, D. R. Vardon, P. C. S. John, N. S. Cleveland, G. Dominick, J. R. Elmore and N. Grundl, *Joule*, 2019, **3**, 1523–1537.
6 N. A. Rorrer, S. F. Notonier, B. C. Knott, B. A. Black, A. Singh, S. R. Nicholson, C. P. Kinchin, G. P. Schmidt, A. C. Carpenter and K. J. Ramirez, *Cell Rep. Phys. Sci.*, 2022, **3**, 100840.
7 R. M. Cywar, N. A. Rorrer, C. B. Hoyt, G. T. Beckham and E. Y.-X. Chen, *Nat. Rev. Mater.*, 2022, **7**, 83–103.
8 L. N. Ornston and R. Y. Stanier, *J. Biol. Chem.*, 1966, **241**, 3776–3786.
9 P. I. Nikel, E. Martínez-García and V. De Lorenzo, *Nat. Rev. Microbiol.*, 2014, **12**, 368–379.
10 P. I. Nikel, M. Chavarría, T. Fuhrer, U. Sauer and V. De Lorenzo, *J. Biol. Chem.*, 2015, **290**, 25920–25932.
11 A. Ankenbauer, R. A. Schäfer, S. C. Viegas, V. Pobre, B. Voß, C. M. Arraiano and R. Takors, *Microb. Biotechnol.*, 2020, **13**, 1145–1161.
12 Y. Okamura-Abe, T. Abe, K. Nishimura, Y. Kawata, K. Sato-Izawa, Y. Otsuka, M. Nakamura, S. Kajita, E. Masai, T. Sonoki and Y. Katayama, *J. Biosci. Bioeng.*, 2016, **121**, 652–658.
13 Y. Suzuki, Y. Otsuka, T. Araki, N. Kamimura, E. Masai, M. Nakamura and Y. Katayama, *Bioresour. Technol.*, 2021, **337**, 125489.
14 A. Z. Werner, W. T. Cordell, C. W. Lahive, B. C. Klein, C. A. Singer, E. C. D. Tan, M. A. Ingraham, K. J. Ramirez, D. H. Kim, J. N. Pedersen, C. W. Johnson, B. F. Pfleger, G. T. Beckham and D. Salvachúa, *Sci. Adv.*, 2023, **9**, eadj0053.
15 K. P. Sullivan, A. Z. Werner, K. J. Ramirez, L. D. Ellis, J. R. Bussard, B. A. Black, D. G. Brandner, F. Bratti, B. L. Buss and X. Dong, *Science*, 2022, **378**, 207–211.
16 A. Z. Werner, R. Clare, T. D. Mand, I. Pardo, K. J. Ramirez, S. J. Haugen, F. Bratti, G. N. Dexter, J. R. Elmore and J. D. Huenemann, *Metab. Eng.*, 2021, **67**, 250–261.
17 N. Mosier, C. Wyman, B. Dale, R. Elander, Y. Y. Lee, M. Holtzapple and M. Ladisch, *Bioresour. Technol.*, 2005, **96**, 673–686.
18 S. Bello, I. Salim, G. Feijoo and M. T. Moreira, *Environ. Sci. Pollut. Res.*, 2021, **28**, 27345–27361.
19 J.-P. Meijnen, J. H. D. Winde and H. J. Ruijssenaars, *Appl. Environ. Microbiol.*, 2008, **74**, 5031–5037.
20 S. Le Meur, M. Zinn, T. Egli, L. Thöny-Meyer and Q. Ren, *BMC Biotechnol.*, 2012, **12**, 53.
21 P. Dvořák and V. de Lorenzo, *Metab. Eng.*, 2018, **48**, 94–108.
22 I. Bator, A. Wittgens, F. Rosenau, T. Tiso and L. M. Blank, *Front. Bioeng. Biotechnol.*, 2020, **7**, 480.
23 J. R. Elmore, G. N. Dexter, D. Salvachúa, M. O'Brien, D. M. Klingeman, K. Gorday, J. K. Michener, D. J. Peterson, G. T. Beckham and A. M. Guss, *Metab. Eng.*, 2020, **62**, 62–71.
24 C. Ling, G. L. Peabody, D. Salvachúa, Y.-M. Kim, C. M. Kneucker, C. H. Calvey, M. A. Monninger, N. M. Munoz, B. C. Poirier and K. J. Ramirez, *Nat. Commun.*, 2022, **13**, 1–14.
25 Y. Wang, F. Horlamus, M. Henkel, F. Kovacic, S. Schläfle, R. Hausmann, A. Wittgens and F. Rosenau, *GCB Bioenergy*, 2019, **11**, 249–259.
26 P. Dvořák, B. Burýšková, B. Popelářová, B. E. Ebert, T. Botka, D. Bujdoš, A. Sánchez-Pascuala, H. Schöttler, H. Hayen, V. de Lorenzo, L. M. Blank and M. Benešík, *Nat. Commun.*, 2024, **15**, 2666.
27 S. C. Mokwatlo, B. C. Klein, P. T. Benavides, E. C. D. Tan, C. M. Kneucker, C. Ling, C. A. Singer, R. Lyons, V. Sànchez i Nogué, K. V. Hestmark, M. A. Ingraham, K. J. Ramirez, C. W. Johnson, G. T. Beckham and D. Salvachúa, *Green Chem.*, 2024, **26**, 10152–10167.
28 C. S. López-Garzón and A. J. J. Straathof, *Biotechnol. Adv.*, 2014, **32**, 873–904.
29 A. Flores, X. Wang and D. R. Nielsen, *Curr. Opin. Biotechnol.*, 2019, **57**, 82–87.

30 A. Eggert, T. Maßmann, D. Kreyenschulte, M. Becker, B. Heyman, J. Büchs and A. Jupke, *Sep. Purif. Technol.*, 2019, **215**, 463–472.
31 J. Pastoors, A. Deitert, C. Michel, K. Günster, M. Finger, J. Hofstede, J. Deischter, A. Biselli, J. Viell, R. Palkovits, A. Jupke and J. Büchs, *Biotechnol. Biofuels Bioprod.*, 2023, **16**, 181.
32 S. Tönjes, E. Uitterhaegen, P. De Brabander, E. Verhoeven, T. Delmulle, K. De Winter and W. Soetaert, *Biochem. Eng. J.*, 2023, **190**, 108746.
33 J. Iyyappan, G. Baskar, B. Bharathiraja and M. Gopinath, *Bioresour. Technol.*, 2020, **308**, 123259.
34 Q. Li, D. Wang, G. Hu, J. Xing and Z. Su, *Biochem. Eng. J.*, 2011, **56**, 150–157.
35 K. Zhang and S.-T. Yang, *Biochem. Eng. J.*, 2015, **96**, 38–45.
36 Y. Zhang, H. Liu, X. Liu, H. Zhu, T. Fan, L. Deng and F. Wang, *Biochem. Eng. J.*, 2020, **160**, 107610.
37 P. Wang, Y. Wang and Z. Su, *Appl. Biochem. Biotechnol.*, 2012, **166**, 974–986.
38 H. Wu, O. Olokede, S.-C. Hsu, S. Roy and M. Holtzapple, *J. Cleaner Prod.*, 2022, **367**, 133000.
39 M. A. Mirata, D. Heerd and J. Schrader, *Process Biochem.*, 2009, **44**, 764–771.
40 R. E. Parales and C. S. Harwood, *J. Bacteriol.*, 1993, **175**, 5829–5838.
41 T. Sonoki, M. Morooka, K. Sakamoto, Y. Otsuka, M. Nakamura, J. Jellison and B. Goodell, *J. Biotechnol.*, 2014, **192**, 71–77.
42 K. A. P. Payne, M. D. White, K. Fisher, B. Khara, S. S. Bailey, D. Parker, N. J. W. Rattray, D. K. Trivedi, R. Goodacre, R. Beveridge, P. Barran, S. E. J. Rigby, N. S. Scrutton, S. Hay and D. Leys, *Nature*, 2015, **522**, 497–501.
43 J. M. Rand, T. Pisithkul, R. L. Clark, J. M. Thiede, C. R. Mehrer, D. E. Agnew, C. E. Campbell, A. L. Markley, M. N. Price, J. Ray, K. M. Wetmore, Y. Suh, A. P. Arkin, A. M. Deutschbauer, D. Amador-Noguez and B. F. Pfleger, *Nat. Microbiol.*, 2017, **2**, 1624–1634.
44 H. J. Kim, B. C. Kim, H. Park, G. Cho, T. Lee, H. T. Kim, S. K. Bhatia and Y.-H. Yang, *J. Biotechnol.*, 2024, **395**, 161–169.
45 G. J. Bentley, N. Narayanan, R. K. Jha, D. Salvachúa, J. R. Elmore, G. L. Peabody, B. A. Black, K. Ramirez, A. De Capite and W. E. Michener, *Metab. Eng.*, 2020, **59**, 64–75.
46 H. Song, Y. Li and Y. Wang, *Eng. Microbiol.*, 2023, **3**, 100051.
47 T. Eng, D. Banerjee, A. K. Lau, E. Bowden, R. A. Herbert, J. Trinh, J.-P. Prahl, A. Deutschbauer, D. Tanjore and A. Mukhopadhyay, *Metab. Eng.*, 2021, **66**, 229–238.
48 B. J. Hritzko, M. J. Ortiz-Vega and N. H. L. Wang, *Ind. Eng. Chem. Res.*, 1999, **38**, 2754–2764.
49 K. W. Staggs and D. R. Nielsen, *Process Biochem.*, 2015, **50**, 1487–1498.
50 D. Salvachúa, P. O. Saboe, R. S. Nelson, C. Singer, I. McNamara, C. del Cerro, Y.-C. Chou, A. Mohagheghi, D. J. Peterson, S. Haugen, N. S. Cleveland, H. R. Monroe, M. T. Guarnieri, E. C. D. Tan, G. T. Beckham, E. M. Karp and J. G. Linger, *Cell Rep. Phys. Sci.*, 2021, **2**, 100587.
51 M. Cheng, X. Xie, P. Schmitz and L. Fillaudeau, *Sep. Purif. Technol.*, 2021, **265**, 118293.
52 E. D. Jensen, F. Ambri, M. B. Bendtsen, A. A. Javanpour, C. C. Liu, M. K. Jensen and J. D. Keasling, *Microb. Biotechnol.*, 2021, **14**, 2617–2626.
53 E. Kuatsjah, C. W. Johnson, D. Salvachúa, A. Z. Werner, M. Zahn, C. J. Szostkiewicz, C. A. Singer, G. Dominick, I. Okekeogbu, S. J. Haugen, S. P. Woodworth, K. J. Ramirez, R. J. Giannone, R. L. Hettich, J. E. McGeehan and G. T. Beckham, *Metab. Eng.*, 2022, **70**, 31–42.
54 D. R. Vardon, N. A. Rorrer, D. Salvachúa, A. E. Settle, C. W. Johnson, M. J. Menart, N. S. Cleveland, P. N. Ciesielski, K. X. Steirer and J. R. Dorgan, *Green Chem.*, 2016, **18**, 3397–3413.
55 L. Han, P. Liu, J. Sun, Y. Wu, Y. Zhang, W. Chen, J. Lin, Q. Wang and Y. Ma, *Sci. Rep.*, 2015, **5**, 13435.
56 M. E. Beber, M. G. Gollub, D. Mozaffari, K. M. Shebek, A. I. Flamholz, R. Milo and E. Noor, *Nucleic Acids Res.*, 2021, **50**, D603–D609.
57 A. Srivastava, P. K. Roychoudhury and V. Sahai, *Biotechnol. Bioeng.*, 1992, **39**, 607–613.
58 K. Schügerl and J. Hubbuch, *Curr. Opin. Microbiol.*, 2005, **8**, 294–300.
59 C. W. Johnson and G. T. Beckham, *Metab. Eng.*, 2015, **28**, 240–247.
60 K.-H. Choi, A. Kumar and H. P. Schweizer, *J. Microbiol. Methods*, 2006, **64**, 391–397.
61 C. R. Amendola, W. T. Cordell, C. M. Kneucker, C. J. Szostkiewicz, M. A. Ingraham, M. Monninger, R. Wilton, B. F. Pfleger, D. Salvachúa, C. W. Johnson and G. T. Beckham, *Metab. Eng.*, 2024, **81**, 88–99.
62 X. Chen, E. Kuhn, E. W. Jennings, R. Nelson, L. Tao, M. Zhang and M. P. Tucker, *Energy Environ. Sci.*, 2016, **9**, 1237–1245.
63 H. M. Alt, A. F. Benson, S. J. Haugen, M. A. Ingraham, W. E. Michener, S. P. Woodworth, K. J. Ramirez and G. T. Beckham, *protocols.io*, 2024. DOI: **10.17504/protocols.io.5qpvob7y9l4o/v2**.